Multi-scale model updating of a timber footbridge using experimental vibration data

Rafael Castro-Triguero[a], Enrique García-Macías[b], Erick I. Saavedra Flores[c,*], Michael I. Friswell[d], Rafael Gallego[e]

[a]*Dept. of Mechanics, University of Cordoba, Campus de Rabanales, 14071 Cordoba, Spain*
[b]*Department of Continuum Mechanics , School of Engineering, University of Seville , Seville , Spain*
[c]*Departamento de Ingeniería en Obras Civiles, Universidad de Santiago de Chile, Av. Ecuador 3659, Estación Central, Santiago, Chile*
[d]*College of Engineering, Swansea University, Swansea SA2 8PP, UK*
[e]*Dept. Structural Mechanics and Hydraulic Engineering, University of Granada, 18071 Granada, Spain*

Abstract

Purpose - The purpose of this paper is to capture the actual structural behaviour of the longest timber footbridge in Spain by means of a multi-scale model updating approach in conjunction with ambient vibration tests.
Design/methodology/approach - In a first stage, a numerical pre-test analysis of the full bridge is performed.This approach offers a first structural model in which optimal sensor placement (OSP) methodologies are applied in order to improve the system identification process. In particular, the Effective Independence (EFI) method is employed to determine the optimal locations of a set of sensors. Ambient vibration tests are conducted to determine experimentally the modal characteristics of the structure. The identified modal parameters are compared with those values obtained from this preliminary model. In order to improve the accuracy of our numerical predictions, the material response is modeled by means of a homogenization-based multi-scale computational approach. In a second stage, the structure is modeled by means of three-dimensional solid elements with the above material definition, capturing realistically the full orthotropic mechanical properties of wood. A Genetic Algorithm (GA) technique is adopted to calibrate the micro-mechanical parameters which are either not well-known or susceptible to considerable variations when measured experimentally.
Findings - An overall good agreement is found between the results of our updated numerical simulations and the corresponding experimental measurements. The longitudinal and transverse Young's moduli, sliding and rolling shear moduli, density and natural frequencies are computed by the present approach. The obtained results reveal the potential predictive capabilities of the present GA/multi-scale/experimental approach to capture accurately the actual behaviour of complex materials and structures.
Originality/value - The uniqueness and importance of this structure leads to an intensive study of its structural behavior. Ambient vibration tests are carried out under environmental excitation. Extraction of modal parameters are obtained from output-only experimental data. The EFI methodology is applied for the OSP on a large-scale structure. Information coming from several length scales, from sub-micrometer dimensions to macroscopic scales, is included in the material definition. The strong differences found between the stiffness along the longitudinal and transverse directions of wood lumbers are incorporated in the structural model. A multi-scale model updating approach is carried out by means of a GA technique to calibrate the micro-mechanical parameters which are either not well-known or susceptible to considerable variations when measured experimentally.

keywords Timber footbridge, multi-scale finite element model, ambient vibration, optimal sensor placement, model updating.
Paper type Research paper.

1. Introduction

The Montoro footbridge (Fig. 1(a)) with a total length of 125.30 m is currently claimed to be the longest wooden footbridge in Spain. It is located in the south of Spain, at Montoro (Córdoba), and crosses the Guadalquivir river.

In recent years structural engineers have focused public attention on the need for improved footbridge monitoring and maintenance [11, 62, 66]. All of these studies analyzed the dynamic response of these civil engineering structures under crowd induced loading. In particular, walking behaviour can interact with the structure and produces problems of resonance. Zivanovic et al. [66] reported a detailed review about vibration serviceability of footbridges under human-induced excitation. This literature survey identified humans as the most important source of vibration for footbridges. This paper highlighted that, of all vibration properties of the footbridge, damping is the most uncertain but is an extremely important parameter as the resonant behaviour tends to govern the vibration serviceability of footbridges. Bujnak et al. [11] illustrated the importance of management, maintenance and reconstruction of footbridge structures. The importance of imperfections, potentially reducing safety and load carrying capacity, was also reported. Van Nimmen et al. [62] studied the methodology of two current codes of practice, the French Sétra guideline and the European guideline HiVoSS, both widely applied in engineering practice. In both evaluation procedures, it is assumed that the dynamical characteristics of the structure, e.g. the natural frequencies, mode shapes, and damping factors, are known. For these reasons, the vibration properties of footbridges are of vital importance in the structural design process.

Numerous examples of vibration-based condition monitoring of bridges are readily found in the literature. Most of them are related to road or railway bridges [2, 10, 20, 24, 35, 37, 39, 48]. In most of the cases modal analysis is carried out to determine the modal parameters of the structure. In particular, operational modal analysis is applied using output-only modal identification methodologies to identify modal parameters during ambient excitation. The modern trend to construct light and slender footbridges has highlighted the importance of the dynamics of such structures. Moschas and Stiros [43] described the measurement and analysis of the deflections of a short-span pedestrian bridge in Athens, analyzed on the basis of geodetic techniques. A comparison between design and real ('as built') dynamic and static characteristics of the footbridge was presented. Bayraktar et al. [7] studied ambient vibration tests of a 18.40 m span steel footbridge located in Trabzon, Turkey. The footbridge consists of a concrete slab, stairs, scarecrows, and piers. The paper focused on the structural evaluation of the footbridge using both numerical and experimental parameters. The modal vibration based assessment of the Podgorica footbridge over the Moraca River in Podgorica, capital of Montenegro, was investigated by Zivanovic et al. [67]. This paper describes this lively full-scale footbridge, its numerical modelling and dynamic testing by modal analysis. Zivanovic et al. [68] then proposed the finite element model updating of the Podgorica footbridge. It was found that even a

*Corresponding author.
Email address: erick.saavedra@usach.cl (Erick I. Saavedra Flores)

very detailed initial finite element model underestimated the natural frequencies of all seven experimentally identified modes of vibration. The ambient vibration-based assessment of the Morca suspension footbridge was studied by Gentile and Gallino [25]. This footbridge, dating back to 1928, links the small city of Morca to the main road crossing the Sesia river (northern Italy). The experimental investigation was preceded by the development of a 3D FE model, where some uncertain parameters of the model were updated to enhance the match between theoretical and experimental natural frequencies. Ivorra et al. [34] studied the dynamic behavior of a pedestrian bridge in Alicante, Spain, which showed vertical and horizontal vibration problems. The natural frequencies, mode shapes, and modal damping factors of the bridge were calculated based on accelerations recorded at different points of the bridge and under different conditions, i.e. ambient vibration and forced vibration produced by a fixed number of pedestrians walking on the bridge at a certain speed and frequency. Caetano et al. [12, 13] studied the human-induced vibration of the Pedro e Ins footbridge at Coimbra, Portugal. The first article describes the studies undertaken at the design stage and the results of a thorough experimental assessment of the constructed bridge properties. The second article discusses the strategy adopted in the design and assessment of the efficiency of a vibration control system. The effects of the changing ambient temperature of the Dowling Hall footbridge was studied by Moaveni and Behmanesh [42]. The footbridge was equipped with a continuous monitoring system that recorded vibration and temperature of the structure. The identified natural frequencies showed significant variability with changing ambient temperature. Hu et al. [30] considered the feasibility of applying a vibration based damage detection approach, based on Principal Component Analysis (PCA), to eliminate environmental effects for the Pedro e Ins footbridge, Portugal.

However, monitoring of timber bridges have received much less research attention. Stiros and Moschas [57] studied the lateral deflections of a timber pedestrian bridge in Patras, Greece. By using a robotic total station (RTS), the authors found a drop of 1.6 Hz in the natural frequencies of the bridge between 2007 and 2008 and then a gradual drop of approximately 8% between 2008 and 2012. The hygro-thermal response of a glulam beam of a pedestrian bridge located in Lisbon, Portugal, was simulated by Fortino et al. [23]. A 3D multi-Fickian numerical method was proposed to integrate the sensor-based hygro-thermal monitoring of timber bridges. The authors highlighted the need to extend their approach to incorporate the mechanical response of timber elements under the service life of bridges. The monitoring of the moisture content of a block-laminated timber bridge was also investigated by Tannert et al. [59]. Very recently, the monitoring of a long-span cable-stayed timber bridge was also investigated by Saracoglu and Bergstrand [55]. Particular attention was paid on the environmental effects on the bridge.

In spite of the above valuable research works, we must note that studies on the vibration performance of timber bridges are still very limited, particularly when considering the influence of the anisotropic mechanical response of wood and its micromechanics on the structural behavior. We remark here that the anisotropy of microstructural phases may play a crucial role in determining both the effective as well as local response of the material [46].

In the present work, we adopt a homogenization-based multi-scale constitutive framework to model the mechanical response of wood in the structural elements of the timber footbridge of Montoro. By using this approach, several features of wood micromechanics are included in our numerical simulations at multiple length scales. The modeling strategy incorporates information coming from three interlinked spatial scales. These are the ultrastructural scale (at the level of nanometers), the mesoscopic (or intermediate) scale (at the order of micrometers) and the macroscopic or structural scale (of the order of meters). In order to collect reliable

information about the actual behavior of the structure, ambient vibration tests were conducted in situ. For this purpose, optimal sensor placement (OSP) techniques were applied to program the measurements. This set of techniques requires a preliminary modal parameters of the structure. Thus, a preliminary FEM defined by beam elements and isotropic constitutive relationships was implemented. Once the experimental data was post-processed, the considerable differences with the preliminary values highlight the limitations of these type of models to predict the dynamic properties of timber footbridges. However, thanks to this experimental base, a more complex anisotropic solid FEM can be implemented. A GA optimization technique is adopted to update those micro-mechanical parameters which are either not well-known or subject to considerable variation. Hence, the differences among the experimental and numerical natural frequencies are minimized. The paper is organized as follows, Section 2: description of the structure of the Montoro footbridge; Section 3: numerical model. In this section, the two main different scales of the numerical approach are presented. In Section 3.1 the preliminary and detailed FE modelings are described (structural scale). In Section 3.2 it is described the microscopic scale (ultrastructural ans mesiscopic scales) for the definition of the constitutive relationships of the wood; Section 4: pre-tests obtained by the preliminary FEM in order to plan the field-tests with OSP techniques; Section 5: Field vibration test; Section 6: Model tuning and numerical results; and Section 7: Conclusions.

2. Description of the Montoro wooden footbridge

The studied footbridge crosses the Guadalquivir river as its passes through Montoro, Spain (Fig. 1(a)). The whole structure consists of four longitudinal girders stiffened by two lateral trusses linked at both ends. All the primary members are made of glued laminated timber with strength grade GL28h. The cross section presents a mean width of 2 m (Fig. 2(b)) and is defined by four longitudinal girders with rectangular cross sections of dimensions 0.48 x 0.22 m and 0.36 x 0.22 m, for the upper and lower girders respectively. These girders are connected by two lateral warren-type trusses with constant sections of 0.26 x 0.22 m. The joints between the elements are defined by embedded steel plates fixed with bolts, that ensures the joints are very stiff. The footbridge has a longitudinal length of 125.30 m, divided into five hyperstatic spans of 33.725-10.35-37.5-10.35-33.725 m (Fig. 2(a)). The structure is supported at its two ends, in addition to the two intermediate reinforced concrete piles. The deck has a longitudinal slope of 3.5% and consists of a first group of small transverse members laying on a second set of beams rotated by 30^o with respect to the longitudinal axis of the bridge (Fig. 1(b),1(c)). The stiffness contribution of these two groups of beams is negligible when compared to the primary structure.

The bridge was constructed in 2010, and partial damage present in the lamination of some members of the footbridge (such as fiber separation) has been confirmed after a visual inspection of the structure. Damage tolerance in engineering structures has been reported, for instance, in [21]. The apparent damage seems not to compromise the whole structural integrity. However, it is not clear whether this assumption is correct or not. Thus, a rigorous modeling of the structure along with field tests are needed in order to assess the actual state of the structure at present, as well as to develop a basis for future assessments with Structural Health Monitoring (SHM) techniques [31, 32].

(a) Montoro bridge over the Guadalquivir river

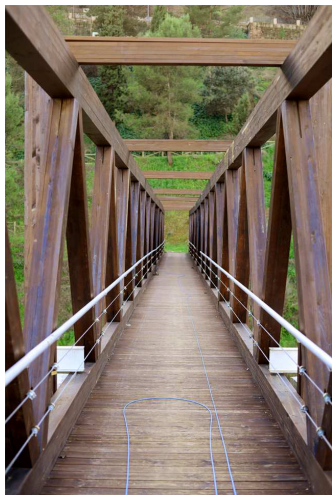

(b) Cross section

(c) Deck detail

Figure 1: General view and details of the bridge structure.

3. The numerical model

3.1. Macroscopic scale

3.1.1. Preliminary FE modeling of the Montoro footbridge

As a first approach, a preliminary 3D model of the footbridge was developed using the commercial finite element software ANSYS 15 [5] (Fig. 3). The type of element chosen for this analysis was the linear (two-noded) BEAM188 with six degrees of freedom per node. The element is based on Timoshenko beam theory (shear deformation effects are included). We note here that the standard beam element formulation can not capture the full multi-dimensional stress-strain state developed in a highly anisotropic material, like wood. Nevertheless, the use of this type of element is not very expensive in terms of computational memory requirements and CPU times so it is usually chosen in the daily practice of structural engineering and therefore, it is a good approach to carry out preliminary simulations. At this stage, we ignore eccentricities found among the longitudinal axes of adjacent structural members. All the connections between two or more members were modeled as rigid joints. The deck was

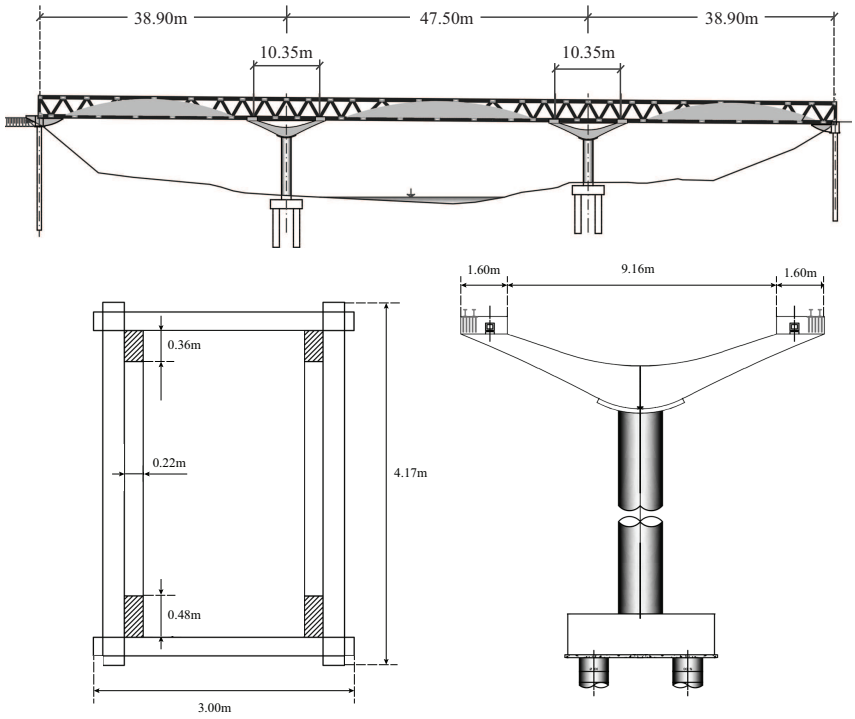

(b) Coss-section

Figure 2: Elevation, coss section and pile geometry of the Montoro bridge.

not explicitly modeled due to its small contribution to the overall stiffness of the structure but its mass was incorporated to the model by means of lumped mass elements called MASS21 in ANSYS, located at the level of the deck.

The footbridge's structure is made of glued laminated timber whose mechanical properties are obtained from the original structural design project [44]. Here, an isotropic material behavior was assumed, with a Young's modulus of 12.6 GPa, a Poisson's ratio of 0.2, and a density of 500 kg/m^3. Fixed boundary conditions were assumed at one end of the bridge, and rollers at the remaining supports.

The numerical results obtained by means of this simplified model represent a first approximation to the structural behaviour of the footbridge. The main idea behind this approach is to build a sufficiently simple model to determine the optimal location of a limited number of sensors on the structure in order to ensure the reliability of the modal data acquired from the vibration-based monitoring process (which is described later, in Section 4).

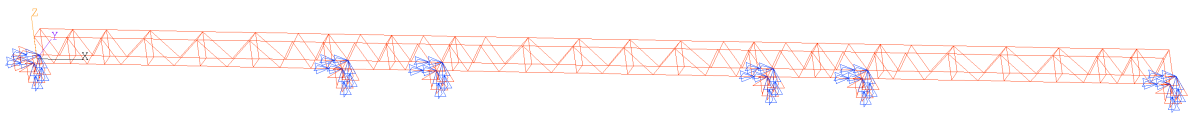

Figure 3: Preliminary 3D beam model of the bridge

3.1.2. Detailed FE modeling of the Montoro footbridge

In a second stage, a detailed 3D model was created using hexahedral solid finite elements. The type of element chosen in ANSYS was SOLID186, which exhibits quadratic displacement behavior. The element is defined by 20 nodes having three translational degrees of freedom per node. The main justification of adopting this type of element is that 3D solid elements are able to capture the full 3D stress-strain state developed in an orthotropic material. The macroscopic mechanical response of wood is defined by 9 material constants which are calculated by the computational homogenization scheme described in Section 3.2. Attention was paid to the orientation of the material principal axes in order to align the wood fibre direction with the longitudinal axis of each structural member.

The finite element mesh consisted of 27920 hexahedral elements and 244538 nodes (Fig. 4).

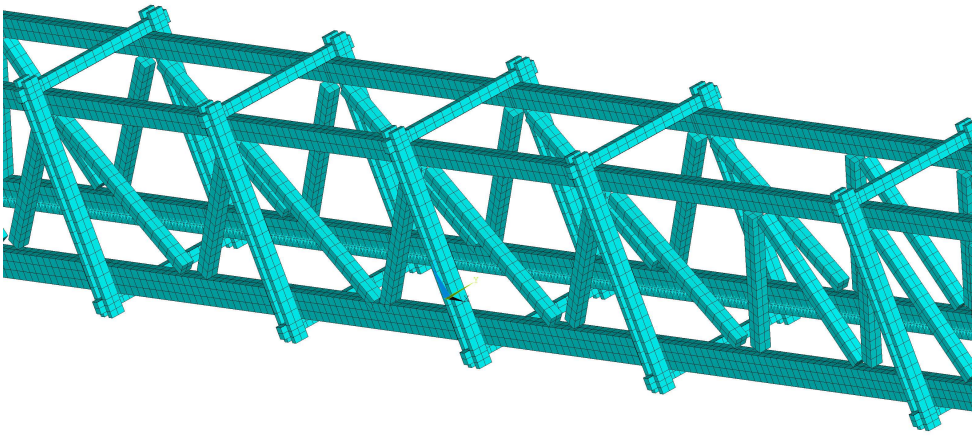

Figure 4: Detailed 3D solid FE model of the bridge

The deck was also modeled by means of MASS21 type elements. Eccentricities between two (or more) member axes at joints were naturally introduced in the model by the use of 3D solid elements. This feature allowed us to reproduce better the actual stiffness of each connection. Nevertheless, in some cases it was necessary to define a set of coupling equations among the degrees of freedom of those nodes located at the ends of converging members at some joints (for instance, between adjacent diagonals and main girders). By following this approach, we circumvented the physical modeling of those connections in which several members of different cross-sections converge at a common point (which proves to be a challenge for the modeling of structures). Thus, we avoided a possibly large number of degrees of freedom associated with the modeling of these connections, along with an excessive number of highly distorted elements. Finally, the definition of the boundary conditions was similar to that described in Section 3.1.1. However, in this new model the boundary conditions were imposed by restraining the displacements to supporting surfaces, equivalent to the area of a neoprene bearing.

3.2. Microscopic scales: Multi-scale material modeling

The computational homogenization scheme adopted to compute the anisotropic constitutive response of wood corresponds to the periodic boundary displacement fluctuations model typically associated with the modeling of (heterogeneous) periodic media [16, 50–52].

In the present multi-scale constitutive theory it is assumed that the macroscopic or homogenised strain tensor at any arbitrary point of the macroscopic continuum is the volume average of the microscopic strain tensor field over the domain of a representative volume element (RVE) of the material. The RVE is such that its microscopic characteristic dimensions are assumed to be much smaller than the macroscopic characteristic length of each structural member, and at the same time, large enough to capture the microscopic heterogeneities in an averaged sense. The present numerical scheme was implemented in ANSYS.

The procedure adopted here consists of modeling the mechanical response of timber by means of two fundamental spatial scales. These are the smallest or ultrastructural scale and the mesoscopic or intermediate scale. The homogenisation of these two scales provides the material law to be used in all of our FE simulations of the footbridge at the macroscopic or structural scale (which is represented by the 3D solid model described in Section 3.1.2).

3.2.1. Ultrastructural scale

The ultrastructural or smallest scale is represented by the wood cell-wall, of the order of a few nanometers. At this level, wood contains three fundamental constituents: cellulose, hemicellulose and lignin. These basic constituents are considered to be universal, with properties inherent to all wood species [29]. The cellulose is a long and stiff polymeric fibre organised into crystalline and amorphous regions which alternate periodically along its length. The length of each crystalline cellulose portion, L_{cc}, varies between 26.5 and 36.4 nm [3]. This periodic arrangement is further covered by an outer surface made up of amorphous cellulose. The crystalline cellulose's width is about 3.2 nm [4], and the total width of the cellulose fibres (including the crystalline core and the outer amorphous sheeting) is 3.6 nm [22]. The degree of cellulose crystallinity, f_{cc}, is defined as the volume fraction of the crystalline portion of cellulose with respect to the total volume of cellulose, and varies between 45 and 60% [4, 14]. The volume fraction of (crystalline and amorphous) cellulose with respect to the total volume of cell-wall, f_c, ranges between 30 and 50% [9, 60]. Hemicellulose is a polymer with little strength built up of sugar units, with mechanical properties highly sensitive to moisture changes. The volume fraction of hemicellulose, f_h, with respect to the total volume of cell-wall, varies between 25 and 29% [56]. Lignin is an amorphous and hydrophobic polymer whose purpose is to cement the individual cells together and to provide shear strength.

These three fundamental constituents form a spatial arrangement called a microfibril which can be represented as a periodic unit building block of rectangular cross-section as shown in Fig. 5.

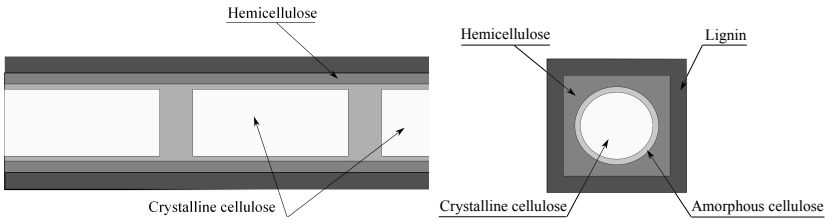

(a) Longitudinal view (b) Transversal view

Figure 5: Schematic representation of a typical microfibril (not to scale). Note that crystalline and amorphous cellulose regions alternate periodically along the length of the microfibril.

A typical FE mesh of the RVE chosen to describe the mechanical response of the microfibril

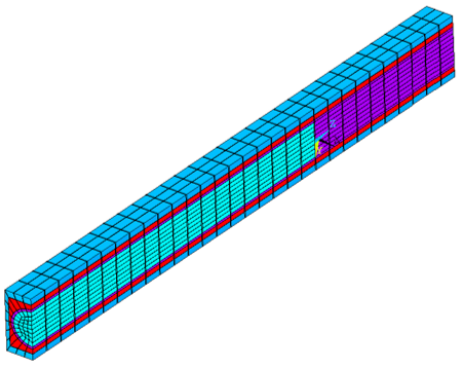

Figure 6: Typical finite element mesh of the microfibril RVE at the smallest scale considered in this study. For the sake of clarity, only one half of the mesh is shown here.

(called here the microfibril RVE) is shown in Fig. 6. For the sake of clarity, only one half of the geometry is shown here. The mesh consists of 4495 nodes and 3960 SOLID186 hexahedral elements.

The mechanical properties of each of the basic constituents considered in our study are summarised in Table 1. This set of data corresponds to an equilibrium moisture content of

Constituent and its mechanical properties	**Value**
Crystalline cellulose	
Longitudinal Young's modulus, E_L^{cc} (GPa)	134
Transversal Young's modulus, E_T^{cc} (GPa)	27.2
Shear modulus, G_{LT}^{cc} (GPa)	4.4
Poisson ratio, ν_{LT}^{cc}	0.1
Amorphous cellulose	
Young's modulus, E^{ac} (GPa)	10.42
Poisson ratio, ν^{ac}	0.23
Hemicellulose	
Longitudinal Young's modulus, E_L^h (GPa)	2
Transversal Young's modulus, E_T^h (GPa)	0.8
Shear modulus, G_{LT}^h (GPa)	1
Poisson ratio, ν_{LT}^h	0.2
Lignin	
Longitudinal Young's modulus, E_L^l (GPa)	2
Transversal Young's modulus, E_T^l (GPa)	1
Shear modulus, G_{LT}^l (GPa)	0.6
Poisson ratio, ν_{LT}^l	0.3

Table 1: Summary of the elastic mechanical properties of the fundamental constituents of wood adopted in all our multi-scale FE simulations [18, 53].

12% and are considered to be constants for all our multi-scale FE simulations.

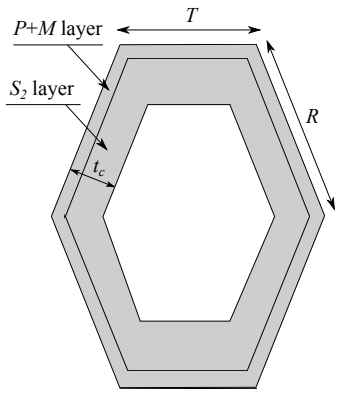

Figure 7: Schematic representation of a wood cell with hexagonal cross-section.

3.2.2. Mesoscopic scale

At the mesoscopic or intermediate scale, of the order of tens to hundreds of micrometers, wood is composed mainly of an arrangement of long slender tubular cells, oriented nearly parallel to the axis of the stem and firmly cemented together. The cross-sections of the wood cells are (normally) hexagonal, and can be defined by means of four geometric parameters: T, R, θ and tc, as shown in Fig. 7. The parameters T and R correspond to the cell dimensions along the tangential and radial directions (of the fibres in the tree trunk). The length T varies between 23 and 30 μm and the length R between 30 and 40 μm [58]; the value of the angle θ ranges between 10 and 18^o [58, 64]; and the cell-wall thickness tc between 3 and 8 μm [58, 64]. We remark that the consideration of the cell-wall geometry is vital for the modelling of closed-cell foam materials [19], like wood. A growth ring is typically formed by 71% of earlywood and 29% of latewood [54].

Depending on the proportions of the constituents and the specific orientation of the microfibrils with respect to the cell axis, that is, the *microfibril angle* (*MFA*), the wall of wood cells can be divided into the compound middle lamella (P+M), which is characterized by a significant abundance of lignin (and therefore of shear strength), and the secondary layer (S), which is formed in turn by the layers S_1, S_2 and S_3. Among all these layers, the S_2 is the thickest and most influential factor in the mechanical behaviour of wood cells. It comprises about 80 – 90% of the total volume of cell-wall [29] and concentrates a high content of cellulose of about 50% in weight [9]. Because of this, we consider the wood cell-wall to be composed of only two layers: the compound middle lamella (P+M), comprising a relative volume of 20%, and the secondary S_2 layer, with a corresponding relative volume of 80%, both with respect to the total volume of cell-wall. Typically, the *MFA* of the S_2 layer varies between 0 and 22^o [61]. We note that most of these microstructural features have been exploited further in order to develop new bio-inspired composite materials [28].

In the present work, the above micromechanical parameters which are defined within a range of variation are considered to be random because of their uncertain value within the indicated range. Such parameters are either not well-known or susceptible to considerable variations when measured experimentally. Table 2 summarizes all these parameters with their corresponding intervals of variation. This information will be used in the optimization scheme described later in this paper.

The P+M layer is assumed to be isotropic because of the random orientation of the *microfibrils* [47]. Its elastic properties are taken from [63]. These correspond to a Young's modulus of 2 GPa and a Poisson's ratio of 0.3. The (orthotropic) mechanical properties of the S_2 layer are

Micromechanical parameter	Interval of variation
Degree of cellulose crystallinity, f_{cc} (%)	45–60
Volume fraction of cellulose, f_c (%)	30–50
Volume fraction of hemicellulose, f_h (%)	25–29
Length of cellulose crystallites, L_{cc} (nm)	26.5–36.4
Radial dimension of wood cell, R (μm)	30–40
Tangential dimension of wood cell, T (μm)	23–30
Cell-wall thickness, t_c (μm)	3–8
Cell angle, θ (^{o})	10–18
Microfibril angle, MFA (^{o})	0–22

Table 2: Summary of the random micro-mechanical parameters chosen for this study and their corresponding intervals of variation [3, 4, 9, 14, 54, 56, 58, 60, 61, 64].

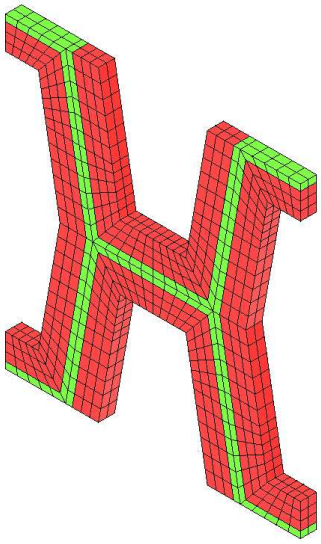

Figure 8: Typical finite element mesh of the wood cell RVE at the intermediate scale.

calculated by means of the computational homogenisation of the cellulose microfibril RVE of Figure 6, taking into account the direction of the cellulose microfibrils according to the *MFA*.

A typical finite element mesh of the RVE chosen to model the wood cell (called here the wood cell RVE) is shown in Fig. 8. The mesh consists of 1917 nodes and 1088 SOLID186 hexahedral elements. Finally, the periodic repetition of the wood cell forms the base (orthotropic) material for the macroscopic scale whose 3D solid FE modeling is detailed in Section 3.1.2.

4. Pre-test analysis

In order to plan the field testing of the structure, the vibration properties of the preliminary numerical model were calculated by performing modal analysis based on iterative eigenvector determination [15]. The structural dynamic characteristics, including the first five modes of vibration, were obtained; the frequencies are shown in Table 3 and the first five mode shapes are shown in Fig. 9. The complex structural configuration results in very complex mode shapes, usually involving simultaneous lateral and vertical displacements. Furthermore, most of the

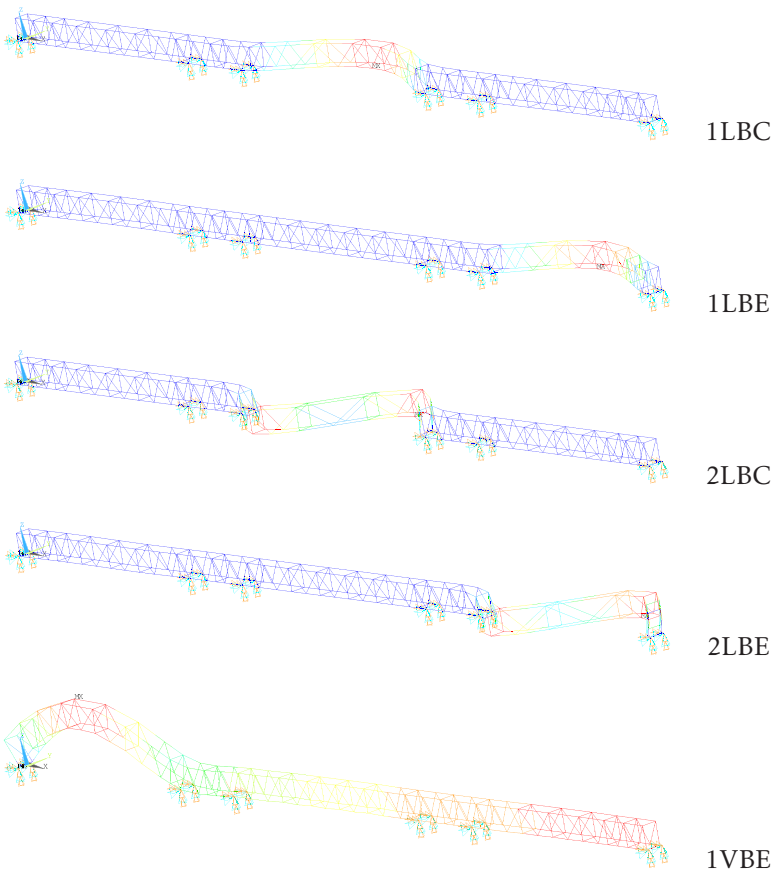

Figure 9: Modes of vibration calculated from the preliminary (beam) FE model

mode shapes are localized and mainly develop in isolated spans because the short spans at the pile supports define a very stiff section.

Mode	Frequency (Hz)	Description of mode shape	Nomenclature
1	0.81	First Lateral/bending mode of central span	1LBC
2	0.97	First Lateral/bending mode of end span	1LBE
3	1.97	Second Lateral/bending mode of central span	2LBC
4	2.24	Second Lateral/bending mode of end span	2LBE
5	6.47	First Vertical/bending mode of end span	1VBE

Table 3: Natural frequencies obtained from the preliminary FE model

It is clear that the structure has a band of modes with low natural frequencies that are also close in frequency and highly coupled; this makes the dynamic features of the structure quite complex.

The optimal placement of a limited number of sensors in a host structure is an important initial step in the field of experimental modal analysis (EMA) and, in particular, in operational modal analysis (OMA). For this reason, a good schedule of the experimental measurements should foresee the appropriate location of sensors in order to ensure an efficient identification of modal properties. Different methodologies have been developed for optimal sensor placement(OSP) [38]. These can be primarily classified into two groups: sub-optimal meth-

ods and methods based on formal optimization strategies. The sub-optimal methods are based on iterative techniques and the latter treat the problem as a classical optimization problem. The method most often employed in practical applications is the Effective Independence (EFI) method introduced by Kammer [36]. The aim of this method is to search for the best set of sensor locations from the set of all candidate locations in the structure, such that the linear independence of the mode shapes is maintained. The starting point of this method is the full modal matrix from a finite element model. All of the degrees of freedom (DOFs) used in the FE model cannot be measured in the real structure due to physical limitations. Therefore, the DOFs corresponding to rotations and coordinates that cannot be measured are eliminated from the full modal matrix. Similarly, not all of the mode shapes can be experimentally measured, and hence some target modes are selected to be optimally detected. Hence, the rows corresponding to DOFs that can be measured are kept and the columns corresponding to target modes are retained in the full modal matrix.

The Fisher information Matrix (FIM) is then defined as

$$\mathbf{FIM} = \phi^T \phi \tag{1}$$

where ϕ is the mode shape matrix (taken from the preliminary numerical model). The FIM matrix has the following properties:

- It is symmetric.
- It is positive semi-definite, that is, its determinant is always positive and all of its the eigenvalues are positive.
- If the column vectors (in this case the mode shapes) are linearly independent, the matrix is full rank, i.e., the rank is equal to the number of the target mode shapes.

If the determinant of the FIM is zero, the columns of the modal matrix (i.e. the target modes) are linearly dependent. Therefore, the purpose of the EFI method is to select the best DOFs (to place the sensors) which maximizes the determinant of the FIM. The DOFs to be eliminated from the modal matrix are chosen in an iterative way. The orthogonal projection matrix E is computed as

$$\mathbf{E} = \phi \mathbf{FIM}^{-1} \phi^T \tag{2}$$

Each element of the diagonal of the matrix **E** represents the fractional contribution of the i^{th} DOF to the rank of this matrix, and in particular to the linear independence of the mode shapes. This is because the matrix **E** is an idempotent matrix whose rank is equal to the sum of the diagonal terms. The selection process can be summarized in the following steps:

1. The DOFs which cannot be measured physically are eliminated. The rows corresponding to DOFs from the modal matrix are deleted.
2. The DOFs which are required a priori for engineering reasons should be retained.
3. Target modes are selected from those of interest. Only the columns from the modal matrix that correspond to those target modes are retained.
4. Matrix **E** is computed. The diagonal of matrix **E** is sorted from the higher elements to the lower ones. The DOF with the lowest value is eliminated from the modal matrix.
5. This process is repeated until the number of DOFs that remain are equal to the desired sensor number of sensors.

6. At every step the FIM determinant (usually represented as the percentage of the initial value) determines the evolution of the process.

7. This procedure for the EFI optimal sensor placement method produces a sub-optimal solution in an iterative way.

Considering the available number of sensors three different setups were chosen to apply in the experimental measurements and are shown in Fig. 10. The first setup, called EFI-Total, was chosen by using the EFI optimal sensor methodology. Two specific setups were also considered to detect the particular behavior of specific spans.

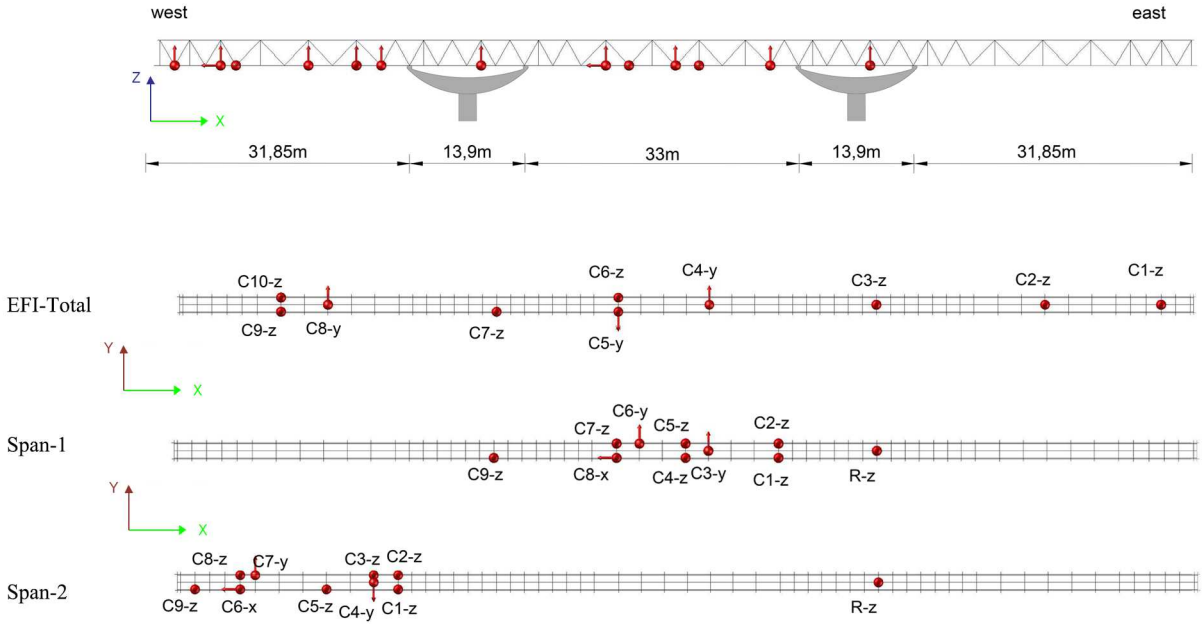

Figure 10: Deck measurement points for different setups: EFI-Total, SPAN-1, and SPAN-2

5. Field vibration test

Ambient vibration tests were conducted on the Montoro bridge to determine its vibration properties. These vibration tests used the three different sensor setups (EFI-Total, SPAN-1, and SPAN-2) detailed in the previous section. For the ambient vibration tests, a LMS Scadas mobile with 16 channels and 24-bit ADC technology controlled by LMS Test.Lab software was employed, as shown in Fig. 5. Two types of accelerometers were considered: 8 PCB seismic accelerometers model 393B31 (PCB Piezotronics, New York, USA) with a sensitivity of 10 V/g ±5%, a broadband resolution of 0.000001 g·rms, a measurement range of 0.5 g peak value, and a frequency range of 0.1 - 200 Hz; and 8 Columbia force balance accelerometers model SA-107BHPC (Columbia Research Laboratories, Pennsylvania, USA) with an output voltage of ± 7.5 Volts, a range of ±0.5 g with a 1 g counterbias, two of them with horizontal sensitivity

(shown in Fig. 11). The time responses were recorded for 15 minutes, and excitations were provided from natural effects (wind, soil movement, river crossing, etc.). Specific data acquisition parameters employed during the ambient vibration tests are detailed in Table 4.

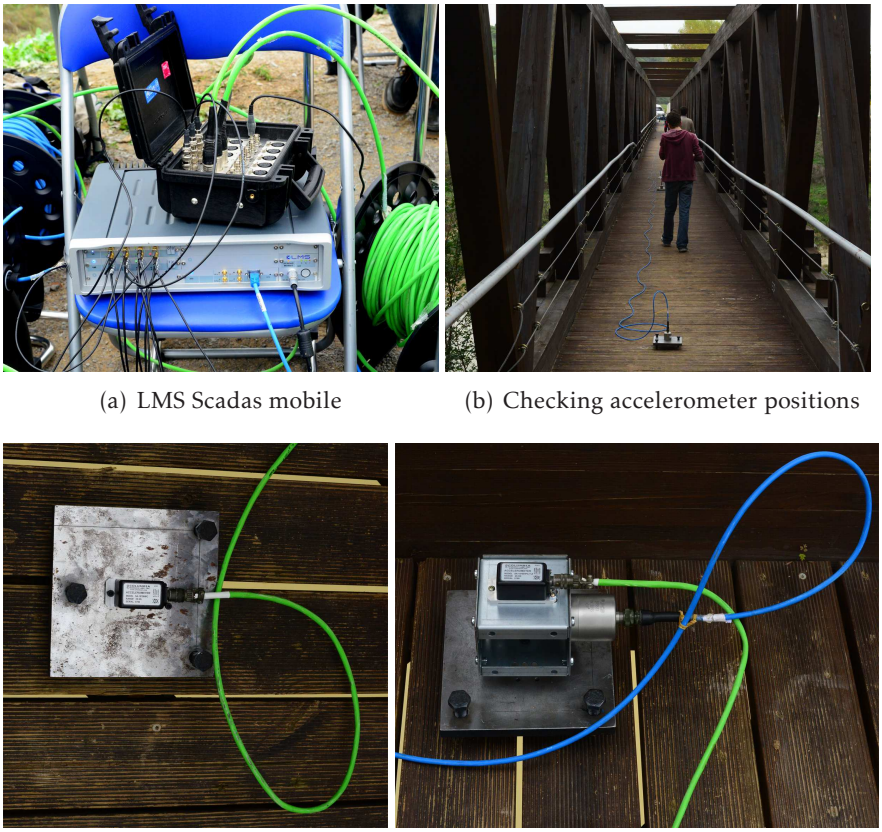

(a) LMS Scadas mobile

(b) Checking accelerometer positions

(c) Force balance accelerometer (SA-107 BHPC)

(d) Cube system for biaxial measurements

Figure 11: Ambient vibration testing and details of accelerometer connections.

Parameter	Value
Max. ADC Bandwidth (Hz)	51200
Bandwidth (Hz)	102.4
Sampling frequency (Hz)	204.8
Filter characteristics	Butterworth (order 6)
Acquisition time (s)	900

Table 4: Data acquisition parameters used for ambient vibration testing

Operational modal analysis (OMA) is based on the assumption that excitation is produced by natural effects, and both the excitation and the recorded accelerations are assumed to be white noise. An example of the time series collected during ambient vibration tests is represented in Fig. 12. It can be observed that the level of excitation in the bridge produced by the ambient excitation is low (of the order of 10^{-3} g). However, this response is sufficient for an efficient system identification. Several system identification algorithms are available in the literature, for example those employed in civil applications include Frequency Domain Decom-

position (FDD), Stochastic System Identification (SSI), and Least-Squares Complex Frequency-domain (LSCF). The LSCF method identifies a so-called common-denominator model and was introduced to find initial values for the iterative maximum likelihood method. The LMS PolyMAX method [45] is a further evolution of the LSCF estimation method and it has been demonstrated that PolyMAX considerably enhances the identification process. The main asset of PolyMAX is that it yields very clear stabilization diagrams with only a very few spurious poles [17]. Hence the LMS PolyMAX system identification method was used to identify the first three natural frequencies by using cross power spectra between recorded measurements (see Fig. 13).

Table 5 shows the natural frequencies measured experimentally. We can observe here significant differences found between these experimental measurements and the numerical results obtained by the preliminary FE beam model. This comparison is made between the same mode shapes, for the EFI-Total setup. The relative errors found between the numerical results coming from this preliminary model and the experimental values are 42, 48 and 46% for the mode shapes 1LBC, 2LBC and 2LBE, respectively. Refer to Table 3 for details on the particular nomenclature used to describe each mode shape.

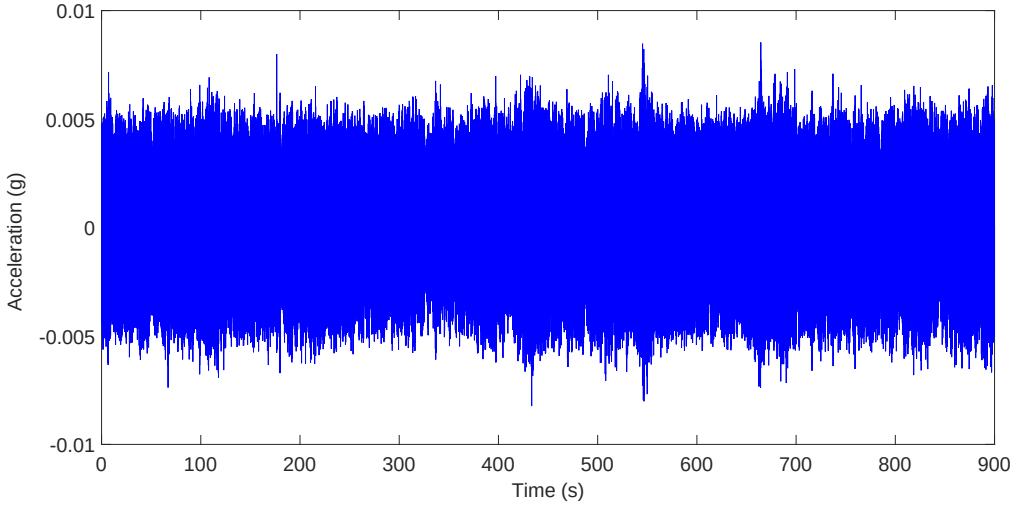

Figure 12: Acceleration time series collected during the ambient vibration test at reference C1-z

Mode	Mode shape	EFI-Total		Span-1		Span-2	
		f (Hz)	ζ (%)	f (Hz)	ζ (%)	f (Hz)	ζ (%)
1	1LBC	1.40	0.64	1.40	0.85	-	-
2	2LBC	3.79	0.76	3.77	1.12	3.79	1.90
3	2LBE	4.18	0.18	4.28	0.26	-	-

Table 5: Modal frequencies and damping ratios from vibration parameter estimation.

6. Model tuning and numerical results

As we are interested in improving the predictions of our multi-scale model, we propose an optimization strategy based on a GA technique [41] to calibrate the random micro-mechanical parameters defined in Table 2.

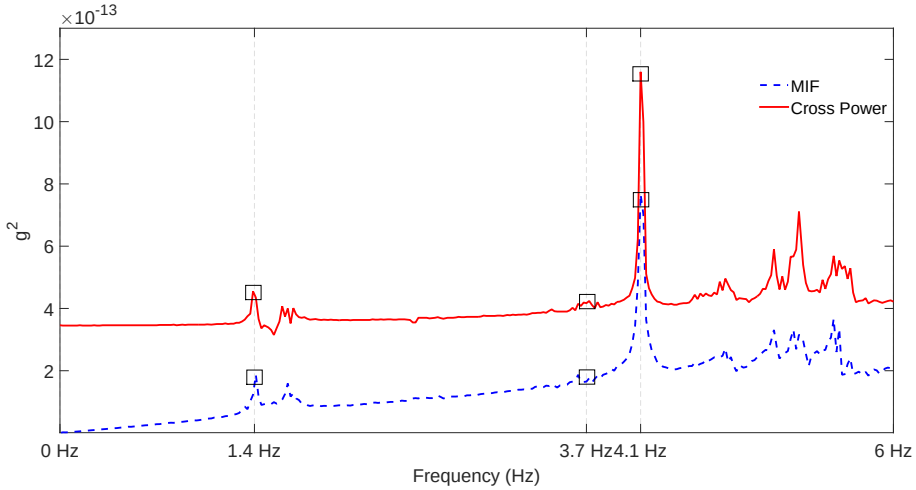

Figure 13: Crosspower estimated from auto-correlation functions and the mode indicator function (MIF)

GAs belong to the larger class of evolutionary algorithms, which generate solutions to optimization problems using techniques inspired by natural evolution, such as inheritance, mutation, selection, and crossover [27]. GAs assume that high-quality parent candidate solutions from different regions in the parameter space can be combined via crossover to produce high-quality offspring candidate solutions. Each individual is characterised by its own genetic code or chromosome, which are represented by real values, generated as a set of values selected within suitable intervals for each optimization parameter [8].

The optimization process starts with the creation of a trial set of micromechanical parameters for each individual according to the genetic methodology, based on the random selection of a value, within the established range, for each parameter being part of the optimization. The performance is estimated by the fitness function which is quantified as the sum of the relative errors between each of the three natural frequencies measured experimentally (shown in Table 5) and their numerical counterparts. Each relative error was calculated as the frequency error normalized by its corresponding experimental frequency. Furthermore, no weighing of the different frequencies was considered. After investigating different convergence criterion, the number of individuals per generation was fixed to 20. Using the Parallel Computing Toolbox in Matlab [40], this optimization problem ran on 8 different processors. This reduced the computational time significantly and allowed us to investigate different convergence criteria. The optimization process was repeated 5 different times to ensure consistency of the outcomes. A cross-over rate of 0.8, which is the default value in Matlab, was adopted. This tends to be the optimum value for typical engineering problems.

Selection, cross-over and mutation operators are all executed to create a new generation starting from the best fit individuals of the previous one. Multiple runs of the same optimization allows the GA to start with different, randomly selected, initial conditions, enabling the analysis a better chance to converge to a global optimum [8].

We emphasise here that the GA is not proposed as the best optimization method nor are the results accepted as the global optimum solution. The GA is used to tune the model parameters in order to improve our numerical predictions.

The GA is applied on our multi-scale model by following a bottom-up approach. That is, at each GA iteration, the algorithm seeks candidate solutions of individuals at the ultrastructural and mesoscopic RVE levels. With a preliminary set of micromechanical parameters at

hand, the computational homogenization process is performed at the (bottom) ultrastructural scale, delivering the effective mechanical properties for the next (upper) mesoscopic scale. The homogenization is repeated again at the the mesoscopic RVE level in order to produce the effective material properties for the simulations which involve the macroscopic solid FE model. The fitness value is computed at the end of each iteration of the GA search until convergence is reached. The criterion adopted to stop the optimization process is to set a tolerance of 0.05 to the average change in the value of the fitness function.

Figure 14 shows the variation of the best and average fitness values as the number of gen-

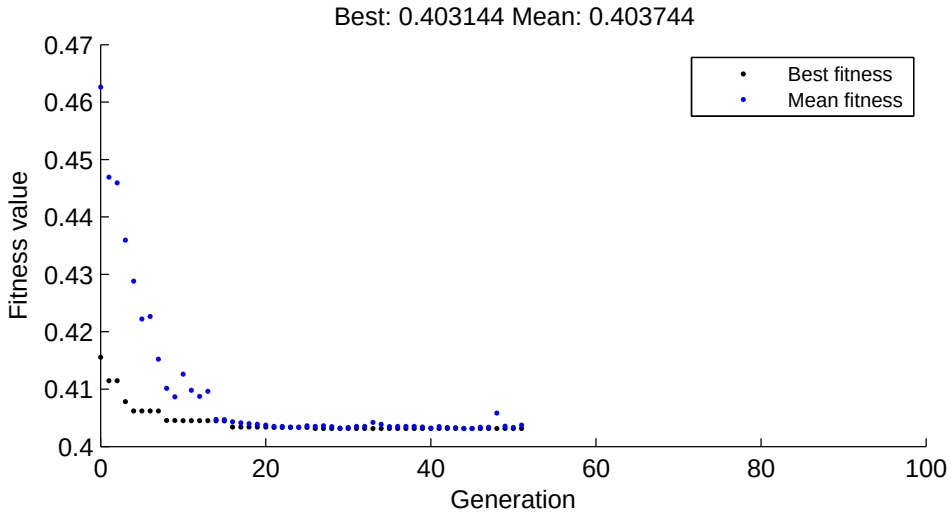

Figure 14: Best and average fitness during optimization.

erations increases. The optimization finishes at the 51^{th} generation.

Once the GA is completed, the chromosomes of the best fit individuals are selected. At this point, the optimization scheme delivers the specific values of the micromechanical parameters so that the differences found between the experimental measurements and our numerical predictions are minimized. Table 6 lists the final values of the optimized micromechanical parameters.

Micromechanical parameter	**Optimal value**
Degree of cellulose crystallinity, f_{cc} (%)	55.59
Volume fraction of cellulose, f_c (%)	48.87
Volume fraction of hemicellulose, f_h (%)	27.65
Length of cellulose crystallites, L_{cc} (nm)	34.98
Radial dimension of wood cell, R (μm)	37.89
Tangential dimension of wood cell, T (μm)	27.09
Cell-wall thickness, t_c (μm)	4.87
Cell angle, θ (^{o})	10.00
Microfibril angle, MFA (^{o})	0.22

Table 6: Optimal values of micromechanical parameters optimized by the GA.

By adopting the above values in our multi-scale material model we obtain a set of nine (orthotropic) constants which are shown in Table 7. Here, the 3-axis represents the longitudinal

Macromechanical properties	Value
E_1 (GPa)	0.123
E_2 (GPa)	1.018
E_3 (GPa)	5.885
G_{12} (GPa)	0.128
G_{23} (GPa)	0.484
G_{13} (GPa)	0.204
ν_{12}	0.144
ν_{23}	0.062
ν_{13}	0.007

Table 7: Orthotropic macromechanical properties obtained by updating the multi-scale 3D solid FE model.

direction of wood fibres.

As one of the purposes of this study is to investigate the actual anisotropic properties of the wood found in the footbridge, we proceed to model a 3D solid beam made of the above material properties and subject to three point bending (simulation not shown here). By analyzing this model, we obtain an updated longitudinal effective Young's modulus of 13.15 GPa. We note that the above Young's modulus is close to the (isotropic) value of 12.6 GPa adopted in the original structural design (which was prepared with glued laminated timber members of strength grade GL28h [26]) and in the preliminary beam FE model. A similar analysis, but with the material principal axes rotated in 90^o, allows us to determine a transverse effective Young's modulus of 0.31 GPa, which is near the design value of 0.42 GPa reported for the same structural strength class [26]. We remark here that these material properties have been computed numerically by updating our multi-scale modeling approach with data obtained from ambient vibration tests.

The fact that the longitudinal and transversal (numerical) Young's moduli approach the corresponding design values allow us to confirm that the structure is not significantly damaged to compromise the elastic properties of the material.

In addition, we studied the sliding and rolling shear modulus (G_o and G_r, respectively) [65] for a timber specimen subject to shear loads. The modelling (not shown here) consisted of applying a linearly-increasing displacement field in a 4-cm-thick parallelepiped-shaped specimen. For the sliding shear modulus, the displacements were applied in the longitudinal direction of wood fibres, producing angular distortion (uniform shear strain) in the plane formed by the longitudinal axis and the thickness direction. We measured the applied shear strain and the resulting shear stress, and with this information we calculated the sliding shear modulus. The rolling shear modulus was computed similarly, but the displacements were applied in the direction perpendicular to wood fibres, producing shear strains in the plane perpendicular to the longitudinal axis of wood fibres.

For these two numerical tests, we obtained a G_o of 315.1 MPa and a G_r of 105.76 MPa. We note that the corresponding value of G_r is within the range of 50 and 200 MPa reported by Aicher and Dill-Langer [1]. Furthermore, the density updated by means of the present approach is 548.8 kg/m^3, which is almost 10% greater than the density of 500 kg/m^3 adopted in the preliminary beam FE model.

Table 8 shows the first 6 natural frequencies obtained from the preliminary and the updated solid FE model in comparison with the experimental results obtained by ambient testing. The

need for more sophisticated FE models which take into account the anisotropic constitutive relationships from a multi-scale analysis is also graphically highlighted in Fig. 15. The better fitting between the experimental and analytic frequencies for the solid FEM points out the great importance of anisotropy in this type of structures.

Mode	Mode shape	Exp. (EFI)	Model 1: Preliminary FEM	Model 2: Updated solid FEM
1	1LBC	1.40	3.04	1.89
2	1LBE	-	3.26	1.99
3	1LBE	-	3.51	2.13
4	2LBE	-	-	3.7
5	2LBC	3.79	5.92	3.79
6	2LBE	4.18	6.03	3.97

Table 8: Numerical frequencies (Hz) obtained by ambient testing (EFI), preliminary FEM and updated solid FEM.

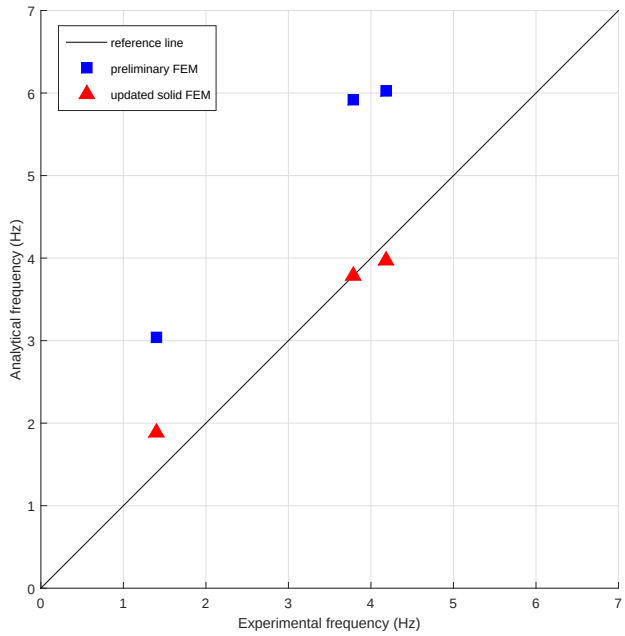

Figure 15: Pairing of experimental and analytical frequencies obtained by the preliminary FEM and the updated solid FEM.

As expected, we can observe a reasonably good agreement with those experimental results shown in Table 5 when the same mode shapes are compared. In this comparison we take those experimental frequencies associated with the EFI-Total setup. Our first numerical frequency reveals a difference of 35% with respect to the first experimental frequency, corresponding to the mode shape 1LBC (refer to Table 3 for details on the particular nomenclature used to describe each mode shape). A perfect agreement is found between the fifth numerical frequency and the second experimental frequency, corresponding to the mode shape 2LBC. Our sixth numerical frequency shows a 5% of difference with respect to the third experimental frequency, corresponding to the mode shape 2LBE. We can also observe that the updated solid FE model delivers significantly better results than those values predicted by the preliminary beam model.

In order to investigate the impact of the actual anisotropic properties of wood on the numerical results, we also show in Table 8 those frequencies (f_{iso}) obtained by assuming an isotropic material behavior in the solid FE model. For this purpose, we skip the computational homogenization process (at the microscopic scales) and we input directly to the (macroscopic) solid FE model an isotropic Young's modulus of 12.6 GPa and a Poisson's ratio of 0.2. To make consistent comparisons, we adopt in this model the same updated density of 548.8 kg/m^3. The observed numerical results show great differences between both models. The frequencies obtained from the isotropic model are almost 60% greater (in average) than those frequencies obtained from the updated (multi-scale) model.

7. Conclusions

A multi-scale modeling strategy was proposed to investigate the modal response of a timber footbridge. The multi-scale framework took material information coming from sub-micrometer dimensions up to the macroscopic scale. The structural behaviour was monitored experimentally using ambient vibration testing. An OSP methodology was adopted to determine the location of sensors and several measurements were carried out in order to ensure the data accuracy. The number of measurement points was limited to the number of accelerometers employed. The PolyMax system identification algorithm was used to extract the modal parameters from the ambient data. The modal parameters obtained experimentally were compared with FE simulations. A first preliminary model was developed by means of standard beam elements and with an isotropic material whose mechanical properties were obtained from the original structural design. Furthermore, a second model was elaborated with 3D solid elements. The material properties considered here were computed numerically by means of the proposed multi-scale modeling approach. A model updating process based on a GA technique was adopted to improve the predictions of the multi-scale 3D solid FE model. By following this optimization scheme, uncertain micro-mechanical parameters of the material were calibrated (within a real range of possible values) in order to capture the actual behavior of the structure.

The present multi-scale approach enabled to capture the strong anisotropy found between the longitudinal and transversal directions of wood lumbers. Great differences were found between the results produced by an isotropic solid 3D model and the updated (anisotropic) multi-scale model, highlighting the importance to consider the anisotropic effects of wood in the modeling process. The analysis of the numerical results allowed us to conclude that the structure does not show signs of significant damage. Finally, the overall good agreement found between the results of our updated numerical simulations and the corresponding experimental measurements reveals the potential predictive capabilities of the present GA/multi-scale/experimental approach to capture accurately the actual behaviour of complex materials and structures.

Acknowledgments

E.I. Saavedra Flores acknowledges the financial support from the Chilean National Commission for Scientific and Technological Research (CONICYT), FONDECYT REGULAR research project No 1140245.

References

[1] Aicher, S., Dill-Langer, G., 2000. Basic considerations to rolling shear modulus in wooden boards. Otto-Graf-Journal 11, 157–165.

[2] Altunisik, A., Bayraktar, A., Sevim, B., zdemir, H., 2011. Experimental and analytical system identification of eynel arch type steel highway bridge. Journal of Constructional Steel Research 67, 1912–1921.
[3] Andersson, S., 2006. A study of the nanostructure of the cell wall of the tracheids of conifer xylem by x-ray scattering. Ph.D. thesis, University of Helsinki, Finland.
[4] Andersson, S., Wikberg, H., Pesonen, E., Maunu, S. L., Serimaa, R., 2004. Studies of crystallinity of scots pine and norway spruce cellulose. Trees - Structure and Function 18 (3), 346–353.
[5] ANSYS, 2013. Parametric Design Language Guide. Release 15.0. ANSYS, Inc., Canonsburg, PA 15317, http://www.ansys.com.
[6] Australian/New Zealand Standard, 2001. AS/NZS 4787. Timber-Assessment of drying quality. Australia-New Zealand.
[7] Bayraktar, A., Altunisik, A., Sevim, B., Trker, T., 2010. Ambient vibration tests of a steel footbridge. Journal of Nondestructive Evaluation 29, 14–24.
[8] Bilgen, O., Saavedra Flores, E. I., Friswell, M. I., 2012. Implementation of a continuous-inextensible-surface piezocomposite airfoil. In: 53rd AIAA/ASME/ASCE/AHS/ASC Structures, Structural Dynamics and Materials Conference. Honolulu, Hawaii.
[9] Bodig, J., Jayne, B., 1982. Mechanics of wood and wood composites. Von Nostrand Reinhold, New York.
[10] Brownjohn, J., Moyo, P., Omenzetter, P., Lu, Y., 2003. Assessment of highway bridge upgrading by dynamic testing and finite-element model updating. Journal of Bridge Engineering 8 (3), 162–172.
[11] Bujnak, J., Hlinka, R., Odrobinak, J., Vican, J., 2012. Diaupdating and evaluation of footbridges. Procedia Engineering 40, 56–61.
[12] Caetano, E., Cunha, A., Magalhaes, F., Moutinho, C., 2010. Studies for controlling human-induced vibration of the pedro e ins footbridge, portugal. part 1: Assessment of dynamic behavior. Engineering Structures 32, 1069–1081.
[13] Caetano, E., Cunha, A., Moutinho, C., Magalhaes, F., 2010. Studies for controlling human-induced vibration of the pedro e ins footbridge, portugal. part 2: Implementation of tuned mass dampers. Engineering Structures 32, 1082–1091.
[14] Castro-Triguero, R., Saavedra Flores, E. I., DiazDelaO, F. A., Friswell, M. I., Gallego, R., 2014. Optimal sensor placement in timber structures by means of a multiscale approach with material uncertainty. Structural Control and Health Monitoring. Accepted for publication.
[15] Chandra, Y., Chowdhury, R., Scarpa, F., Adhikari, S., Sienz, J., Arnold, C., Murmu, T., Bould, D., 2012. Vibration frequency of graphene based composites: A multiscale approach. Materials Science and Engineering: B 177 (3), 303 – 310.
[16] Chandra, Y., Scarpa, F., Chowdhury, R., Adhikari, S., Sienz, J., 2013. Multiscale hybrid atomistic-fe approach for the nonlinear tensile behaviour of graphene nanocomposites. Composites Part A: Applied Science and Manufacturing 46, 147 – 153.
[17] Chellini, G., Nardini, L., Liu, K., Reynders, E., Peeters, B., De Roeck, G., Salvatore, W., Sorrentino, G., Tisalvi, M., 2008. Experimental dynamic analysis of the sesia viaduct, a composite high-speed railway bridge. In: Proceedings of IMAC 26, Orlando, FL., USA.
[18] Chen, W., Lickfield, G. C., Yang, C. Q., 2004. Molecular modeling of cellulose in amorphous state. part i: model building and plastic deformation study. Polymer 45 (3), 1063–1071.
[19] Chen, Y., Das, R., Battley, M., 2015. Effects of cell size and cell wall thickness variations on the stiffness of closed-cell foams. International Journal of Solids and Structures 52, 150 – 164.
[20] Cury, A., Cremona, C., Dumoulin, J., 2012. Long-term monitoring of a psc box girder bridge: Operational modal analysis, data normalization and structural modification assessment. Mechanical Systems and Signal Processing 33, 13–37.
[21] Das, R., Jones, R., 2015. Characteristics of the design surface of damage tolerance parameters and their relation to shape optimisation. International Journal of Fatigue 70, 490 – 502.
[22] Donaldson, L. A., Singh, A. P., 1998. Bridge-like structures cellulose microfibrils. Holzforschung 52 (5), 449–454.
[23] Fortino, S., Genoese, A., Genoese, A., Nunes, L., Palma, P., 2013. Numerical modelling of the hygro-thermal response of timber bridge during their service life: A monitoring case-study. Construction and Building Materials 47, 1225–1234.
[24] Frangopol, D., Strauss, A., Kim, S., 2008. Bridge reliability assessment based on monitoring. Journal of Bridge Engineering 13 (3), 258–270.
[25] Gentile, C., Gallino, N., 2008. Ambient vibration testing and structural evaluation of an historic suspension footbridge. Advances in Engineering Software 39, 356–366.
[26] GLULAM, 2010. Structural glued laminated timber - Design essentials. Glued Laminated Timber Association, 2010.
[27] Goldberg, D., 1989. Genetic Algorithms in search, optimization and machine learning. Addison-Wesley.

[28] Haldar, S., Gheewala, N., Grande-Allen, K., Sutton, M., Bruck, H., 2011. Multi-scale mechanical characterization of palmetto wood using digital image correlation to develop a template for biologically-inspired polymer composites. Experimental Mechanics 51 (4), 575–589.
[29] Hofstetter, K., Hellmich, C., Eberhardsteiner, J., 2005. Development and experimental validation of a continuum micromechanics model for the elasticity of wood. European Journal of Mechanics A/Solids 24 (6), 1030–1053.
[30] Hu, W., Moutinho, C., Caetano, E., Magalhaes, F., Cunha, A., 2012. Continuous dynamic monitoring of a lively footbridge for serviceability assessment and damage detection. Mechanical Systems and Signal Processing 33, 38–55.
[31] Inman, D. J., Farrar, C. R., Lopes, V., Steffen, V., 2005. Damage Prognosis: For Aerospace, Civil and Mechanical Systems. John Wiley & Sons, Ltd.
[32] Inman, D. J., Grisso, B. L., 2007. Chapter1: Adaptive Structures for Structural Health Monitoring. John Wiley & Sons, Ltd, pp. 1–32.
[33] INN – Instituto Nacional de Normalización, 2006. NCh 1198. Madera. Construcciones en Madera. Cálculo. Chile.
[34] Ivorra, S., Foti, D., Bru, D., Baeza, F., 2014. Dynamic behavior of a pedestrian bridge in alicante, spain. Journal of Performance of Constructed Facilities.
[35] Kaliyaperumal, G., Imam, B., Righiniotis, T., 2011. Advanced dynamic finite element analysis of a skew steel railway bridge. Engineering Structures 33, 181–190.
[36] Kammer, D. C., 1991. Sensor placement for on-orbit modal identification and correlation of large space structures. Journal of Guidance, Control and Dynamics 14, 251–259.
[37] Kim, H., Kim, N., Jang, J., Kim, Y., 2012. Analysis model verification of a suspension bridge exploiting configuration survey and field-measured data. Journal of Bridge Engineering 17 (5), 794–803.
[38] Li, D. S., Li, H. N., 2006. The state of the art of sensor placement methods in structural health monitoring. In: Tomizuka, M., Yun, C. B., Giurgiutiu, V. (Eds.), Smart Structures and Materials 2006: Sensors and Smart Structures Technologies for Civil, Mechanical, and Aerospace Systems. Vol. 6174. pp. 1217–1227.
[39] Magalhaes, F., Caetano, E., Cunha, A., Flamand, O., Grillaud, G., 2012. Ambient and free vibration tests of the millau viaduct: Evaluation of alternative processing strategies. Engineering Structures 45, 372–384.
[40] MathWorks, 2012. Parallel Computing Toolbox: For Use with MATLAB. User's Guide.
[41] Mitchell, M., 1998. An Introduction to Genetic Algorithms. MIT Press.
[42] Moaveni, B., Behmanesh, I., 2012. Effects of changing ambient temperature on finite element model updating of the dowling hall footbridge. Engineering Structures 43, 56–68.
[43] Moschas, F., Stiros, S., 2014. Three-dimensional dynamic deflections and natural frequencies of a stiff footbridge based on measurements of collocated sensors. Structural Control and Health Monitoring 21, 23–42.
[44] Nevado, M., 2011. Pasarela peatonal Montoro – Documento final de verificacion normativa. Z047.
[45] Peeters, B., Van der Auweraer, H., Vanhollebeke, F., Guillaume, P., 2007. Operational modal analysis for estimating the dynamic properties of a stadium structure during a football game. Shock and Vibration 14 (4), 283–303.
[46] Pina, J. C., Kouznetsova, V. G., Geers, M. G. D., 2015. Thermo-mechanical analyses of heterogeneous materials with a strongly anisotropic phase: the case of cast iron. International Journal of Solids and Structures 63, 153 – 166.
[47] Qing, H., Mishnaevsky Jr., L., 2009. Moisture-related mechanical properties of softwood: 3D micromechanical modeling. Computational Materials Science 46 (2), 310–320.
[48] Ribeiro, D., Calada, R., Delgado, R., Brehm, M., Zabel, V., 2012. Finite element model updating of a bowstring-arch railway bridge based on experimental modal parameters. Engineering Structures 40, 413–435.
[49] Riesco Muñoz, G., Díaz González, J., 2007. Caractersticas físicas de la madera de pino procedente de raleos en el noroeste de España. Maderas, Ciencia y Tecnología 9 (3), 233–244.
[50] Saavedra Flores, E. I., de Souza Neto, E. A., 2010. Remarks on symmetry conditions in computational homogenisation problems. Engineering Computations 27 (4), 551–575.
[51] Saavedra Flores, E. I., DiazDelaO, F. A., Ajaj, R. M., Friswell, M. I., Fernando, G. F., 2014. Mathematical modelling of the stochastic mechanical properties of wood and its extensibility at small scales. Applied Mathematical Modelling 38 (15–16), 3958–3967.
[52] Saavedra Flores, E. I., DiazDelaO, F. A., Friswell, M. I., Ajaj, R. M., 2014. Investigation on the extensibility of the wood cell-wall composite by an approach based on homogenisation and uncertainty analysis. Composite Structures 108, 212–222.
[53] Salmén, L., 2004. Micromechanical understanding of cell-wall structure. Comptes Rendus Biologies 327 (9-10), 873–880.
[54] Salvo, L., Ananías, R., Cloutier, A., 2004. Influencia de la estructura anatómica en la permeabilidad específica transversal al gas del pino radiata. Maderas. Ciencia y Tecnología 6 (1), 33–44.

[55] Saracoglu, E., Bergstrand, S., 2015. Continuous monitoring of a long-span cable-stayed timber bridge. Journal of Civil Structural Health Monitoring 5 (2), 183–194.
[56] Sixta, H., 2006. Handbook of pulp. Volume 1. Wiley-VCH Verlag GmbH & Co.
[57] Stiros, S., Moschas, F., 2014. Rapid decay of a timber footbridge and changes in its modal frequencies derived from multiannual lateral deflection measurements. Journal of Bridge Engineering.
[58] Tang, S., 1998. Modeling the mechanical properties of Pinus Radiata. Master's thesis, University of Canterbury, New Zealand.
[59] Tannert, T., Muller, A., Vogel, M., 2010. Structural health monitoring of timber bridges. In: Malo, K. A., Kleppe, O., Dyken, T. (Eds.), Proceedings of the International Conference Timber Bridges ICB2010. Lillehammer, Norway.
[60] Timell, T., 1982. Recent progress in the chemistry and topochemistry of compression wood. Wood Science and Technology 16 (2), 83–122.
[61] Valenzuela, J., Ulloa, I., Rallo, M., 2003. Estudio del ángulo fibrilar y su relación con la edad cambial en Pinus Radiata D. Don, proveniente de la Séptima Región, Chile. Maderas, Ciencia y Tecnología 5 (2), 117–124.
[62] Van Nimmen, K., Lombaert, G., De Roeck, G., Van den Broeck, P., 2014. Vibration serviceability of footbridges: Evaluation of the current codes of practice. Engineering Structures 59, 448–461.
[63] Watanabe, U., Norimoto, M., 2000. Three dimensional analysis of elastic constants of the wood cell wall. Wood Research 87, 1–7.
[64] Watanabe, U., Norimoto, M., Morooka, T., 2000. Cell wall thickness and tangential young's modulus in coniferous early wood. Journal of Wood Science 46, 109–114.
[65] Zhou, Q., Gong, M., Chui, Y. H., Mohammad, M., 2014. Measurement of rolling shear modulus and strength of cross laminated timber fabricated with black spruce. Construction and Building Materials 64, 379386.
[66] Zivanovic, S., Pavic, A., Reynolds, P., 2005. Vibration serviceability of footbridges under human-induced excitation: a literature review. Journal of Sound and Vibration 279, 1–74.
[67] Zivanovic, S., Pavic, A., Reynolds, P., 2006. Modal testing and fe model tuning of a lively footbridge structure. Engineering Structures 28, 857–868.
[68] Zivanovic, S., Pavic, A., Reynolds, P., 2007. Finite element modelling and updating of a lively footbridge: The complete process. Journal of Sound and Vibration 301, 126–145.